axioms

MDPI

Article

A Truncated-Kernel Mollification Method for the Cauchy Problem of the Modified Helmholtz Equation

Huilin Xu *, Fanli Xu and Baoxia Wang

College of Mathematics and Computer Science, Gannan Normal University, Ganzhou 341000, China
* Correspondence: hlxu@gnnu.edu.cn

Abstract

This paper addresses the Cauchy problem for the multi-dimensional modified Helmholtz equation, a classical and severely ill-posed problem. A truncated-kernel mollification method is proposed as an effective regularization approach. Both the *a priori* and *a posteriori* regularization parameter choice strategies are examined, and the associated error estimates and convergence rates of the regularized solutions are established. The practical viability and effectiveness of the method are further validated through numerical experiments.

Keywords: mollification method; truncated-kernel; modified Helmholtz equation; Cauchy problem

MSC: 65N21; 35R30

1. Introduction

The modified Helmholtz equation models steady-state heat conduction with thermal loss, bioheat transfer in living tissues, and diffusion processes involving absorption or reaction. It further arises in the linearization of the Poisson–Boltzmann equation for electrolyte solutions and in implicit time discretizations of the heat equation. The Cauchy problem for the modified Helmholtz equation, with solutions that exhibit exponential decay, naturally appears in inverse scattering theory and impedance tomography [1,2]. This problem is inherently ill-posed in the Hadamard sense; even small perturbations in the input data can lead to significant instabilities in the corresponding numerical solutions [3]. To mitigate this ill-posedness, significant research efforts in recent years have focused on developing and applying stable numerical methods for solving such Cauchy problems. Notable approaches include the quasi-reversibility method [4], the truncation method [4,5], the quasi-boundary value method [5,6], the Tikhonov-type regularization method [7,8], the adaptive Runge–Kutta method [9], the iterative regularization method [10,11], and the mollification method [12–14], among others.

Among these methods, the mollification method aims to construct stable solutions by smoothing perturbed input data through convolution with suitable kernel functions. This technique has been widely applied to solving Cauchy problems associated with elliptic and parabolic equations [15], inverse source problems [16–18], inverse Schrödinger problems [19,20], inverse Laplace transform problems [21], as well as backward heat problems [22,23]. The choice of kernel functions is of central importance in the mollification method. Widely used kernels include the Dirichlet, Poussin, Gaussian, and Weierstrass kernels, along with many others [15].

Check for updates

Academic Editors: Xinhui Shao, Hailong Shen and Guanyu Xue

Received: 30 June 2026
Revised: 31 July 2026
Accepted: 31 July 2026
Published: 5 August 2026

Copyright: © 2026 by the authors. Licensee MDPI, Basel, Switzerland. This article is an open access article distributed under the terms and conditions of the Creative Commons Attribution (CC BY) license.

This paper aims to apply the mollification method to solve the Cauchy problem associated with a multi-dimensional modified Helmholtz equation:

$$\begin{cases} \Delta w(x,\mathbf{y}) - k^2 w(x,\mathbf{y}) = 0, \ \ 0 < x \le 1, \ \ \mathbf{y} \in \mathbb{R}^n, \\ w(0^+,\mathbf{y}) = f(\mathbf{y}), \ \ \mathbf{y} \in \mathbb{R}^n, \\ w_x(0^+,\mathbf{y}) = g(\mathbf{y}), \ \ \mathbf{y} \in \mathbb{R}^n, \end{cases} \tag{1}$$

where $\Delta = \frac{\partial^2}{\partial x^2} + \sum_{i=1}^{n} \frac{\partial^2}{\partial y_i^2}$ is an $(n+1)$-dimensional Laplace operator and $k > 0$ denotes the wave number. The Cauchy problem consists in determining the solution $w(x,\mathbf{y})$ from the given data $f(\mathbf{y})$ and $g(\mathbf{y})$. In the one-dimensional case, [12] applies the mollification method with the Dirichlet kernel and establishes an *a priori* regularization parameter choice strategy, while [13] proposes an *a priori* strategy using the Poussin kernel for problem (1). Neither [12] nor [13] provides an *a posteriori* strategy for choosing regularization parameters. The *a priori* regularization parameter choice depends on smoothness assumptions concerning the exact solution, whereas the *a posteriori* approach dispenses with them entirely. In the multi-dimensional case, [14] establishes a unified framework for the mollification method, presents both the *a priori* and *a posteriori* regularization parameter choice strategies, and demonstrates that the Dirichlet, Poussin, and Gaussian kernels satisfy the conditions required by this framework. However, the corresponding regularized solution achieves only logarithmic-order convergence. Both the Dirichlet and Poussin kernels belong to the class of truncated-kernel functions [20]. A general form of truncated-kernel functions is presented in this paper. Building upon the classical Dirichlet and Poussin kernels, two new types are devised: the logarithmic-type kernel and the hyperbolic tangent-type kernel. These kernels are then employed to construct a mollification regularization method for the Cauchy problem of the modified Helmholtz equation. Both *a priori* and *a posteriori* parameter choice strategies are proposed, and the corresponding convergence rates are rigorously proven. The resulting power-law rate is shown to be significantly superior to the logarithmic convergence rate attainable in [14]. Numerical experiments show that the proposed method reconstructs both continuous and discontinuous solutions with high accuracy.

The paper is organized as follows. In Section 2, we analyze the ill-posedness of the Cauchy problem and introduce the definition of the truncated-kernel function. In Section 3, we propose *a priori* regularization parameter choice strategies and derive the corresponding error estimates for the regularized solution. In Section 4, we develop *a posteriori* strategies and establish the associated convergence rates. In Section 5, we demonstrate the numerical effectiveness of the proposed method through several numerical examples. Finally, We summarize the main contributions and conclusions of this study.

2. The Truncated-Kernel Mollification Method

To facilitate the analysis, we decompose problem (1) into two sub-problems:

$$\begin{cases} \Delta u(x,\mathbf{y}) - k^2 u(x,\mathbf{y}) = 0, \quad 0 < x \le 1, \quad \mathbf{y} \in \mathbb{R}^n, \\ u(0^+,\mathbf{y}) = f(\mathbf{y}), \quad \mathbf{y} \in \mathbb{R}^n, \\ u_x(0^+,\mathbf{y}) = 0, \quad \mathbf{y} \in \mathbb{R}^n \end{cases} \tag{2}$$

and

$$\begin{cases} \Delta v(x,\mathbf{y}) - k^2 v(x,\mathbf{y}) = 0, \quad 0 < x \le 1, \quad \mathbf{y}\in\mathbb{R}^n, \\ v(0^+,\mathbf{y}) = 0, \quad \mathbf{y}\in\mathbb{R}^n, \\ v_x(0^+,\mathbf{y}) = g(\mathbf{y}), \quad \mathbf{y}\in\mathbb{R}^n. \end{cases} \tag{3}$$

The solution of (1) is $w(x,\mathbf{y}) = u(x,\mathbf{y}) + v(x,\mathbf{y})$. Applying the Fourier transform yields the following results [14]:

$$\hat{u}(x,\xi) = \cosh(x\sqrt{\xi^2+k^2})\hat{f}(\xi), \quad \hat{v}(x,\xi) = \frac{\sinh(x\sqrt{\xi^2+k^2})}{\sqrt{\xi^2+k^2}}\hat{g}(\xi), \tag{4}$$

where the n-dimensional Fourier transform of $f(\mathbf{y})$ is defined as

$$\hat{f}(\xi) := \frac{1}{(2\pi)^{\frac{n}{2}}}\int_{\mathbb{R}^n} e^{-i\xi\mathbf{y}} f(\mathbf{y})d\mathbf{y}, \quad \xi \in \mathbb{R}^n.$$

Consider the perturbed data $f^\delta(\mathbf{y})$ and $g^\delta(\mathbf{y})$ satisfying

$$\|f^\delta - f\| \le \delta, \quad \|g^\delta - g\| \le \delta, \tag{5}$$

where $\|\cdot\|$ denotes the L^2-norm and $\delta > 0$ represents the noise level. The unboundedness of the operator kernel functions $\cosh(x\sqrt{\xi^2+k^2})$ and $\frac{\sinh(x\sqrt{\xi^2+k^2})}{\sqrt{\xi^2+k^2}}$ as $\xi \to \infty$ causes instability in solutions (4); see [3]. To stabilize the inherently unstable solutions, we apply the mollification method with kernel function $\hat{P}_\mu(\xi)$, where $\xi \in \mathbb{R}^n$. The corresponding regularized solutions are given by

$$\hat{u}^{\mu,\delta}(x,\xi) = \cosh(x\sqrt{\xi^2+k^2})\hat{P}_\mu(\xi)\hat{f}^\delta(\xi) \tag{6}$$

and

$$\hat{v}^{\mu,\delta}(x,\xi) = \frac{\sinh(x\sqrt{\xi^2+k^2})}{\sqrt{\xi^2+k^2}}\hat{P}_\mu(\xi)\hat{g}^\delta(\xi), \tag{7}$$

respectively. Consequently, the regularized solution to problem (1) is given by

$$w^{\mu,\delta}(x,\mathbf{y}) = \frac{1}{(2\pi)^{\frac{n}{2}}}\int_{\mathbb{R}^n} e^{i\xi\mathbf{y}}\hat{w}^{\mu,\delta}(x,\xi)d\xi, \tag{8}$$

where

$$\hat{w}^{\mu,\delta}(x,\xi) = \hat{u}^{\mu,\delta}(x,\xi) + \hat{v}^{\mu,\delta}(x,\xi).$$

In this paper, we focuse on truncated-kernel functions satisfying the following definition.

Definition 1. *A kernel function $\hat{P}_\mu(\xi)$, where $\xi \in \mathbb{R}^n$ and $0 < \mu < 1$, that satisfies the following three conditions is defined as a truncated-kernel function:*

(1) $0 \le \hat{P}_\mu(\xi) \le 1, \quad \xi \in \mathbb{R}^n$;

(2) $\sup_{\xi\in\mathbb{R}^n} \hat{P}_\mu(\xi)e^{x|\xi|} \le e^{\frac{cx}{\mu}}, \quad c > 0,\ 0 \le x \le 1$;

(3) $\sup_{\xi\in\mathbb{R}^n}(1-\hat{P}_\mu(\xi))e^{(x-1)|\xi|} \le e^{\frac{x-1}{\mu}}, \quad 0 \le x \le 1.$

Well-known examples of truncated-kernel functions include the Dirichlet kernel

$$\hat{P}_\mu(\xi) = \chi_{\left[-\frac{1}{\mu},\frac{1}{\mu}\right]}(\xi) = \begin{cases} 1, & |\xi| \le \frac{1}{\mu}, \\ 0, & |\xi| > \frac{1}{\mu} \end{cases} \tag{9}$$

and the Poussin kernel

$$\hat{P}_\mu(\xi) = \begin{cases} 1, & |\xi| \le \frac{1}{\mu}, \\ 2-\mu|\xi|, & \frac{1}{\mu} < |\xi| < \frac{2}{\mu}, \\ 0, & |\xi| \ge \frac{2}{\mu}. \end{cases} \tag{10}$$

It can be demonstrated that, for the Dirichlet kernel, the constant c in Definition 1 equals 1*, while for the Poussin kernel, it equals* 2*. A more general form of the truncated-kernel function can be expressed as follows.*

Lemma 1. *Let k be a real-valued function that is continuous and decreasing on* $(1,2)$ *and satisfies* $0 \le k(x) \le 1$ *for all* $x \in (1,2)$*. Then the function*

$$\hat{P}_\mu(\xi) = \begin{cases} 1, & |\xi| \le \frac{1}{\mu}, \\ k(\ \mu|\xi|\ ), & \frac{1}{\mu} < |\xi| < \frac{2}{\mu}, \\ 0, & |\xi| \ge \frac{2}{\mu} \end{cases} \tag{11}$$

is a truncated-kernel function.

Proof. The inequality $0 \le \hat{P}_\mu(\xi) \le 1$ holds for all $\xi \in \mathbb{R}^n$, so it remains only to verify conditions (2) and (3) of Definition 1. For $0 \le x \le 1$, we have

$$\sup_{\xi \in \mathbb{R}^n} \hat{P}_\mu(\xi) e^{x|\xi|} = \sup_{|\xi| < \frac{2}{\mu}} \hat{P}_\mu(\xi) e^{x|\xi|} \le \sup_{|\xi| < \frac{2}{\mu}} e^{x|\xi|} = e^{\frac{2x}{\mu}}$$

which confirms condition (2) for $c = 2$. Similarly, for $0 \le x \le 1$,

$$\sup_{\xi \in \mathbb{R}^n} (1 - \hat{P}_\mu(\xi)) e^{(x-1)|\xi|} = \sup_{\xi > \frac{1}{\mu}} (1 - \hat{P}_\mu(\xi)) e^{(x-1)|\xi|} \le \sup_{\xi > \frac{1}{\mu}} e^{(x-1)|\xi|} \le e^{\frac{x-1}{\mu}}$$

which confirms condition (3). □

Throughout the rest of this paper, we assume that $\hat{P}_\mu(\xi)$ is a truncated-kernel function given by (11), and that $k(x)$ satisfies the condition in Lemma 1. Beyond the specific cases of $k(x) = 0$ for the Dirichlet kernel and $k(x) = 2 - \ x\ $ for the Poussin kernel, various truncated-kernel functions can be constructed by appropriately specifying $k(x)$, $1 < x < 2$. In this paper, we construct two novel truncated-kernel functions. The first is the logarithmic-type kernel; for $m > 0$, the corresponding $k(x)$ is

$$k_1(\ x\ ) = 1 - \frac{1}{m} \ln\big((e^m - 1)(\ x\ - 1) + 1\big), \quad 1 < x < 2.$$

Direct substitution yields $k_1(1) = 1$ and $k_1(2) = 0$. Differentiating yields

$$k_1'(x) = -\frac{1}{m} \frac{e^m - 1}{(e^m - 1)(x - 1) + 1}, \quad 1 < x < 2.$$

Since $k_1'(x) < 0$ for all $x \in (1,2)$, the function $k_1(x)$ is strictly decreasing on $(1,2)$. It follows that $k_1(x)$ satisfies all the conditions of Lemma 1. Moreover, as $k_1'(x)$ is monotonically increasing, the magnitude $|k_1'(x)|$ is monotonically decreasing, indicating that the rate of decrease of $k_1(x)$ diminishes progressively over $(1,2)$. Furthermore, the supremum magnitude of the derivative is

$$\sup_{1 < x < 2} |k_1'(x)| = |k_1'(1)| = \frac{e^m - 1}{m},$$

and since $m > 0$, this supremum magnitude increases strictly with m; consequently, larger m yields a steeper maximal downward slope for $k_1(x)$ on $(1,2)$.

The second is the hyperbolic tangent-type kernel: for $m > 0$,

$$k_2(x) = \frac{1}{2}\left(1 - \frac{\tanh(2m\,x\, - 3m)}{\tanh m}\right), \quad 1 < x < 2.$$

Similarly, $k_2(1) = 1$, $k_2(2) = 0$. Differentiating yields

$$k_2'(x) = -\frac{m}{\tanh m}\operatorname{sech}^2(2mx - 3m), \quad 1 < x < 2$$

and

$$\sup_{1<x<2} |k_2'(x)| = |k_2'(\frac{3}{2})| = \frac{m}{\tanh m}.$$

Since $k_2'(x) < 0$ for all $x \in (1,2)$, the function $k_2(x)$ is strictly decreasing on $(1,2)$. Thus, $k_2(x)$ also satisfies all the conditions of Lemma 1. Moreover, as $k_2'(x)$ is monotonically decreasing on the interval $(1, \frac{3}{2}]$, thus the rate of decrease accelerates monotonically. On the interval$(\frac{3}{2}, 2)$, $k_2'(x)$ is monotonically increasing, so the rate of decrease diminishes monotonically. Consequently, $x = \frac{3}{2}$ is the maximum point of the rate of decrease of $k_2(x)$ over $(1,2)$. Moreover, the supremum magnitude increases strictly with m; consequently, larger m yields a steeper maximal downward slope for $k_2(x)$ on $(1,2)$.

The graphs of the logarithmic-type and hyperbolic tangent-type kernels for different values of m are presented in Figure 1 with $n = 1$ and $\mu = 0.1$.

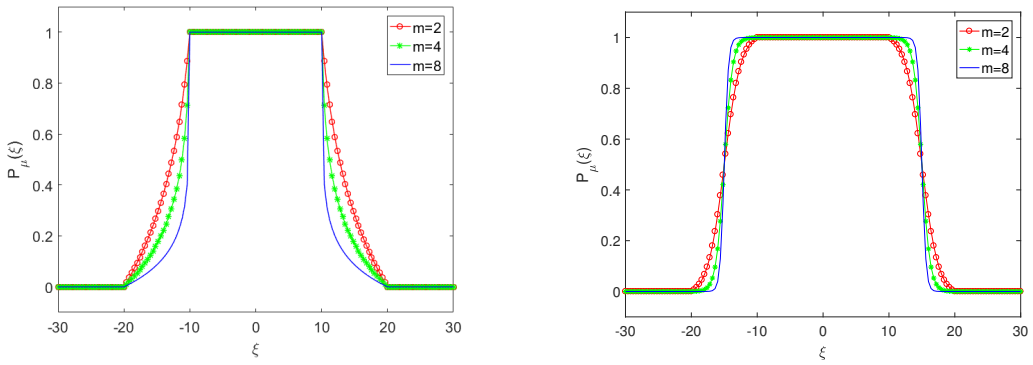


Figure 1. The logarithmic-type kernel (**a**) and the hyperbolic tangent-type kernel (**b**) for different values of m with $n = 1$ and $\mu = 0.1$.

We now present several fundamental properties satisfied by the operator kernel functions given in (4).

Lemma 2. *When $0 < x \leq 1$, the following inequalities hold.*

(1) $\cosh(x\sqrt{\xi^2 + k^2}) \leq e^x\sqrt{\xi^2+k^2}$;

(2) $\cosh(x\sqrt{\xi^2 + k^2}) \geq \frac{1}{2}e^x\sqrt{\xi^2+k^2}$;

(3) $\frac{\sinh(x\sqrt{\xi^2+k^2})}{\sqrt{\xi^2+k^2}} \leq e^x\sqrt{\xi^2+k^2}$;

(4) $\frac{\sinh(x\sqrt{\xi^2+k^2})}{\sqrt{\xi^2+k^2}} \leq \cosh(x\sqrt{\xi^2 + k^2})$;

(5) $\frac{\cosh(x\sqrt{\xi^2+k^2})}{\cosh(\sqrt{\xi^2+k^2})} \leq 2e^{(x-1)}\sqrt{\xi^2+k^2}$;

(6) $\frac{\sinh(x\sqrt{\xi^2+k^2})}{\sinh(\sqrt{\xi^2+k^2})} \leq e^{(x-1)}\sqrt{\xi^2+k^2}$.

Conclusions (1) and (2) are trivial and are therefore omitted for brevity. For the remaining conclusions, the reader is referred to [3].

At the end of this section, we introduce additional stability conditions via the following assumptions on the exact data $f(\mathbf{y})$ and $g(\mathbf{y})$:

$$\|f(\cdot)\|_{M^p(R^n)} \le E_p, \quad \|g(\cdot)\|_{M^p(R^n)} \le E_p. \tag{12}$$

Here, $E_p > 0$ is a fixed constant, and the norm on the space $M^p(\mathbb{R}^n)$ is defined by

$$\|f(\cdot)\|_{M^p(\mathbb{R}^n)} := \left(\int_{\mathbb{R}^n} e^{p|\xi|} |\hat{f}(\xi)|^2 \, d\xi \right)^{1/2}.$$

Remark 1. *When $p = 0$, we have $\|f(\cdot)\|_{M^0(\mathbb{R}^n)} = \|f(\cdot)\|_{L^2(\mathbb{R}^n)}$; when $p > 0$, we have $\|f(\cdot)\|_{M^p(\mathbb{R}^n)} = \|e^{\frac{p}{2}|\xi|} \hat{f}(\xi)\|_{L^2(\mathbb{R}^n)}$.*

3. The *a Priori* Parameter Choice Strategies

In this section, we first consider the case $0 < x < 1$.

Theorem 1. *Assume that $\hat{P}_\mu(\xi)$ is a truncated-kernel function and $w^{\mu,\delta}(x, \mathbf{y})$ denotes the regularized solution defined by (8) for $0 < x < 1$. If condition (5) is satisfied and condition (12) holds for $p = 2$, then the following error estimate holds:*

$$\|w^{\mu,\delta}(x,\cdot) - w(x,\cdot)\| \le 2e^{\frac{x}{\mu}} e^{xk} \delta + 2e^{\frac{x-1}{\mu}} e^{xk} E_2.$$

When $\mu = \frac{1+(c-1)x}{\ln(E_2/\delta)}$, we have

$$\|w^{\mu,\delta}(x,\cdot) - w(x,\cdot)\| \le 4e^{xk} E_2^{\frac{cx}{1+(c-1)x}} \delta^{\frac{1-x}{1+(c-1)x}}. \tag{13}$$

Proof. Applying Parseval's identity and the triangle inequality, we obtain

$$\begin{aligned} \|u^{\mu,\delta}(x,\cdot) - u(x,\cdot)\| &= \|\hat{u}^{\mu,\delta}(x,\cdot) - \hat{u}(x,\cdot)\| \\ &\le \|\hat{u}^{\mu,\delta}(x,\cdot) - \hat{u}^{\mu,0}(x,\cdot)\| + \|\hat{u}^{\mu,0}(x,\cdot) - \hat{u}(x,\cdot)\|, \end{aligned}$$

where

$$\begin{aligned} \|\hat{u}^{\mu,\delta}(x,\cdot) - \hat{u}^{\mu,0}(x,\cdot)\| &= \|\hat{P}_\mu(\xi) \cosh(x\sqrt{\xi^2 + k^2})(\hat{f}^\delta(\xi) - \hat{f}(\xi))\| \\ &\le \sup_{\xi \in \mathbb{R}^n} |\hat{P}_\mu(\xi) \cosh(x\sqrt{\xi^2 + k^2})| \delta \\ &\le \sup_{\xi \in \mathbb{R}^n} |\hat{P}_\mu(\xi) e^{x(|\xi|+k)}| \delta \\ &= \sup_{\xi \in \mathbb{R}^n} |\hat{P}_\mu(\xi) e^{x|\xi|}| e^{xk} \delta \\ &\le e^{\frac{cx}{\mu}} e^{xk} \delta \end{aligned}$$

and

$$\begin{aligned} \|\hat{u}^{\mu,0}(x,\cdot) - \hat{u}(x,\cdot)\| &= \|(1 - \hat{P}_\mu(\xi)) \cosh(x\sqrt{\xi^2 + k^2}) \hat{f}(\xi)\| \\ &= \|(1 - \hat{P}_\mu(\xi)) \cosh(x\sqrt{\xi^2 + k^2}) e^{-|\xi|} e^{|\xi|} \hat{f}(\xi)\| \\ &\le \sup_{\xi \in \mathbb{R}^n} |(1 - \hat{P}_\mu(\xi)) \frac{\cosh(x\sqrt{\xi^2 + k^2})}{e^{|\xi|}}| E_2 \\ &\le \sup_{\xi \in \mathbb{R}^n} |(1 - \hat{P}_\mu(\xi)) e^{(x-1)|\xi|}| e^{xk} E_2 \\ &\le \sup_{\xi \in \mathbb{R}^n} |(1 - \hat{P}_\mu(\xi)) e^{(x-1)|\xi|}| e^{xk} E_2 \\ &\le e^{\frac{x-1}{\mu}} e^{xk} E_2. \end{aligned}$$

Therefore, we have

$$\|u^{\mu,\delta}(x,\cdot) - u(x,\cdot)\| \le e^{\frac{cx}{\mu}} e^{xk}\delta + e^{\frac{x-1}{\mu}} e^{xk} E_2.$$

Analogous to the error estimate of $u^{\mu,\delta}(x,\cdot)$, we can estimate that of $v^{\mu,\delta}(x,\cdot)$.

$$\begin{aligned}\|v^{\mu,\delta}(x,\cdot) - v(x,\cdot)\| &= \|\hat{v}^{\mu,\delta}(x,\cdot) - \hat{v}(x,\cdot)\| \\ &\le \|\hat{v}^{\mu,\delta}(x,\cdot) - \hat{v}^{\mu,0}(x,\cdot)\| + \|\hat{v}^{\mu,0}(x,\cdot) - \hat{v}(x,\cdot)\|,\end{aligned}$$

where

$$\begin{aligned}\|\hat{v}^{\mu,\delta}(x,\cdot) - \hat{v}^{\mu,0}(x,\cdot)\| &= \|\hat{P}_\mu(\xi)\frac{\sinh(x\sqrt{\xi^2+k^2})}{\sqrt{\xi^2+k^2}}(\hat{g}^\delta(\xi) - \hat{g}(\xi))\| \\ &\le \|\hat{P}_\mu(\xi)\cosh(x\sqrt{\xi^2+k^2})(\hat{g}^\delta(\xi) - \hat{g}(\xi))\| \\ &\le \sup_{\xi\in\mathbb{R}^n} |\hat{P}_\mu(\xi)\cosh(x\sqrt{\xi^2+k^2})|\delta \\ &\le e^{\frac{cx}{\mu}} e^{xk}\delta\end{aligned}$$

and

$$\begin{aligned}\|\hat{v}^{\mu,0}(x,\cdot) - \hat{v}(x,\cdot)\| &= \|(1-\hat{P}_\mu(\xi))\frac{\sinh(x\sqrt{\xi^2+k^2})}{\sqrt{\xi^2+k^2}}\hat{g}(\xi)\| \\ &= \|(1-\hat{P}_\mu(\xi))\frac{\sinh(x\sqrt{\xi^2+k^2})}{\sqrt{\xi^2+k^2}}e^{-|\xi|}e^{|\xi|}\hat{g}(\xi)\| \\ &\le \sup_{\xi\in\mathbb{R}^n} |(1-\hat{P}_\mu(\xi))\frac{\cosh(x\sqrt{\xi^2+k^2})}{e^{|\xi|}}|E_2 \\ &\le \sup_{\xi\in\mathbb{R}^n} |(1-\hat{P}_\mu(\xi))e^{(x-1)|\xi|}|e^{xk}E_2 \\ &\le e^{\frac{x-1}{\mu}} e^{xk} E_2.\end{aligned}$$

Consequently, we obtain

$$\|v^{\mu,\delta}(x,\cdot) - v(x,\cdot)\| \le e^{\frac{cx}{\mu}} e^{xk}\delta + e^{\frac{x-1}{\mu}} e^{xk} E_2,$$

and subsequently,

$$\|w^{\mu,\delta}(x,\cdot) - w(x,\cdot)\| \le 2e^{\frac{cx}{\mu}} e^{xk}\delta + 2e^{\frac{x-1}{\mu}} e^{xk} E_2.$$

When $\mu = \frac{1+(c-1)x}{\ln(E_2/\delta)}$, the estimate (13) holds. □

Next, we consider the case $x = 1$. In contrast to the case $0 < x < 1$, stronger additional assumptions on the exact data $f(\mathbf{y})$ and $g(\mathbf{y})$ are required.

Theorem 2. *Assume that $\hat{P}_\mu(\xi)$ is a truncated-kernel function and $w^{\mu,\delta}(x,\mathbf{y})$ denotes the regularized solution defined by (8) at $x = 1$. If condition (5) is satisfied and condition (12) holds for $p > 2$, then the following error estimate holds:*

$$\|w^{\mu,\delta}(1,\cdot) - w(1,\cdot)\| \le 2e^{\frac{c}{\mu}} e^{k}\delta + 2e^{\frac{2-p}{2\mu}} e^{k} E_p.$$

When $\mu = \frac{2c+p-2}{2\ln(E_p/\delta)}$, we obtain

$$\|w^{\mu,\delta}(1,\cdot) - w(1,\cdot)\| \le 4e^{k} E_p^{\frac{2c}{2c+p-2}} \delta^{\frac{p-2}{2c+p-2}}. \tag{14}$$

Proof. Applying Parseval's identity and the triangle inequality, we obtain

$$\begin{aligned}\|u^{\mu,\delta}(1,\cdot)-u(1,\cdot)\| &= \|\hat{u}^{\mu,\delta}(1,\cdot)-\hat{u}(1,\cdot)\| \\ &\le \|\hat{u}^{\mu,\delta}(1,\cdot)-\hat{u}^{\mu,0}(1,\cdot)\|+\|\hat{u}^{\mu,0}(1,\cdot)-\hat{u}(1,\cdot)\|,\end{aligned}$$

where

$$\begin{aligned}\|\hat{u}^{\mu,\delta}(1,\cdot)-\hat{u}^{\mu,0}(1,\cdot)\| &= \|\hat{P}_\mu(\xi)\cosh(\sqrt{\xi^2+k^2})(\hat{f}^\delta(\xi)-\hat{f}(\xi))\| \\ &\le \sup_{\xi\in\mathbb{R}^n}|\hat{P}_\mu(\xi)\cosh(\sqrt{\xi^2+k^2})|\delta \\ &\le e^{\frac{c}{\mu}}e^k\delta\end{aligned}$$

and

$$\begin{aligned}\|u^{\mu,0}(1,\cdot)-u(1,\cdot)\| &= \|\hat{u}^{\mu,0}(1,\cdot)-\hat{u}(1,\cdot)\| \\ &= \|(1-\hat{P}_\mu(\xi))\cosh(\sqrt{\xi^2+k^2})\hat{f}(\xi)\| \\ &\le \|(1-\hat{P}_\mu(\xi))\frac{\cosh(\sqrt{\xi^2+k^2})}{e^{\frac{p}{2}|\xi|}}e^{\frac{p}{2}|\xi|}\hat{f}(\xi)\| \\ &\le \sup_{\xi\in\mathbb{R}^n}|(1-\hat{P}_\mu(\xi))e^{\frac{2-p}{2}|\xi|}|e^kE_p \\ &\le e^{\frac{2-p}{2\mu}}e^kE_p.\end{aligned}$$

Hence, we have

$$\|u^{\mu,\delta}(1,\cdot)-u(1,\cdot)\| \le e^{\frac{c}{\mu}}e^k\delta+e^{\frac{2-p}{2\mu}}e^kE_p.$$

Analogous to the error estimate of $u^{\mu,\delta}(x,\cdot)$, we can derive that of $v^{\mu,\delta}(x,\cdot)$.

$$\begin{aligned}\|v^{\mu,\delta}(1,\cdot)-v(1,\cdot)\| &= \|\hat{v}^{\mu,\delta}(1,\cdot)-\hat{v}(1,\cdot)\| \\ &\le \|\hat{v}^{\mu,\delta}(1,\cdot)-\hat{v}^{\mu,0}(1,\cdot)\|+\|\hat{v}^{\mu,0}(1,\cdot)-\hat{v}(1,\cdot)\| \\ &= \|\hat{P}_\mu(\xi)\frac{\sinh(\sqrt{\xi^2+k^2})}{\sqrt{\xi^2+k^2}}(\hat{g}^\delta(\xi)-\hat{g}(\xi))\| \\ &\quad+\|(1-\hat{P}_\mu(\xi))\frac{\sinh(\sqrt{\xi^2+k^2})}{\sqrt{\xi^2+k^2}}\hat{g}(\xi)\| \\ &\le \sup_{\xi\in\mathbb{R}^n}|\hat{P}_\mu(\xi)\cosh(\sqrt{\xi^2+k^2})|\delta \\ &\quad+\|(1-\hat{P}_\mu(\xi))\frac{\cosh(\sqrt{\xi^2+k^2})}{e^{\frac{p}{2}|\xi|}}e^{\frac{p}{2}|\xi|}\hat{g}(\xi)\| \\ &\le e^{\frac{c}{\mu}}e^k\delta+\sup_{\xi\in\mathbb{R}^n}|(1-\hat{P}_\mu(\xi))e^{\frac{2-p}{2}|\xi|}|e^kE_p \\ &\le e^{\frac{c}{\mu}}e^k\delta+e^{\frac{2-p}{2\mu}}e^kE_p.\end{aligned}$$

Hence, we have

$$\|w^{\mu,\delta}(1,\cdot)-w(1,\cdot)\| \le 2e^{\frac{c}{\mu}}e^k\delta+2e^{\frac{2-p}{2\mu}}e^kE_p.$$

When $\mu=\frac{2c+p-2}{2\ln(E_p/\delta)}$, the estimate (14) holds. □

4. The *a Posteriori* Parameter Choice Strategies

The *a priori* choice strategies for the regularization parameter $\mu = \mu(\delta)$ presented in Theorems 1 and 2 rely on additional assumptions about the exact data $f(\mathbf{y})$ and $g(\mathbf{y})$. However, such assumptions are often difficult to verify in practical applications. Therefore, in this section, we consider *a posteriori* choice strategies for the regularization parameter that do not depend on these prior assumptions. The Morozov discrepancy principle is a widely used *a posteriori* parameter choice strategy [24]. In the following, we propose a modified version of this principle. The parameter $\mu = \mu(\delta)$ in the regularized solution $u^{\mu,\delta}(x, \mathbf{y})$ satisfies

$$d_1(\mu) := \|\hat{P}_\mu(\xi)\hat{f}^\delta(\xi) - \hat{f}^\delta(\xi)\| = \|(1 - \hat{P}_\mu(\xi))\hat{f}^\delta(\xi)\| = \delta + \tau\delta^{\frac{1}{c}}, \tag{15}$$

and the parameter $\mu = \mu(\delta)$ in the regularized solution $v^{\mu,\delta}(x, \mathbf{y})$ satisfies

$$d_2(\mu) := \|\hat{P}_\mu(\xi)\hat{g}^\delta(\xi) - \hat{g}^\delta(\xi)\| = \|(1 - \hat{P}_\mu(\xi))\hat{g}^\delta(\xi)\| = \delta + \tau\delta^{\frac{1}{c}}, \tag{16}$$

where $\tau > 0$ is a given constant such that

$$\delta + \tau\delta^{\frac{1}{c}} < \min\{\|f^\delta(\cdot)\|, \|g^\delta(\cdot)\|\}. \tag{17}$$

Lemma 3. *Assume that $\hat{P}_\mu(\xi)$ is a truncated-kernel function, then $d_1(\mu)$ and $d_2(\mu)$ satisfy the following properties:*

(1) *$d_1(\mu)$ and $d_2(\mu)$ are continuous and increasing functions;*
(2) $\lim\limits_{\mu\to 0^+} d_1(\mu) = \lim\limits_{\mu\to 0^+} d_2(\mu) = 0$;
(3) $\lim\limits_{\mu\to+\infty} d_1(\mu) = \|f^\delta(\cdot)\|$ *and* $\lim\limits_{\mu\to+\infty} d_2(\mu) = \|g^\delta(\cdot)\|$.

Proof. (1) Given that $\hat{P}_\mu(\xi)$ is a truncated-kernel function given by (11), it follows that $d_1(\mu) = \|(1 - \hat{P}_\mu(\xi))\hat{f}^\delta(\xi)\|$ is continuous and increasing in μ.

(2) Since $\lim\limits_{\mu\to 0^+} \hat{P}_\mu(\xi) = 1$ for any $\xi \in \mathbb{R}^n$, it follows immediately that $\lim\limits_{\mu\to 0^+}(1 - \hat{P}_\mu(\xi)) = 0$, and therefore $\lim\limits_{\mu\to 0^+} d_1(\mu) = 0$.

(3) Since $\lim\limits_{\mu\to+\infty} \hat{P}_\mu(\xi) = 0$ for any $\xi \in \mathbb{R}^n$, therefore $\lim\limits_{\mu\to+\infty} d_1(\mu) = \|f^\delta(\cdot)\|$.

The same conclusion applies to $d_2(\mu)$. □

Lemma 3 together with condition (17) ensures the solvability of Equations (15) and (16).

Analogously to the previous section, we first consider the case $0 < x < 1$. To derive the error estimate for the regularized solution, we begin by presenting the following lemmas.

Lemma 4. *Assume that $\mu_1 = \mu_1(\delta)$ and $\mu_2 = \mu_2(\delta)$ are solutions to Equations (15) and (16), respectively. Then, we have*

$$\|\hat{P}_{\mu_1}(\xi)\hat{f}^\delta(\xi) - \hat{f}(\xi)\| \le 2\delta + \tau\delta^{\frac{1}{c}}, \quad \|\hat{P}_{\mu_2}(\xi)\hat{g}^\delta(\xi) - \hat{g}(\xi)\| \le 2\delta + \tau\delta^{\frac{1}{c}}.$$

Proof. Applying the triangle inequality, we obtain

$$\begin{aligned}\|\hat{P}_{\mu_1}(\xi)\hat{f}^\delta(\xi) - \hat{f}(\xi)\| &= \|\hat{P}_{\mu_1}(\xi)\hat{f}^\delta(\xi) - \hat{f}^\delta(\xi) + \hat{f}^\delta(\xi) - \hat{f}(\xi)\| \\ &\le \|\hat{P}_{\mu_1}(\xi)\hat{f}^\delta(\xi) - \hat{f}^\delta(\xi)\| + \delta \\ &\le 2\delta + \tau\delta^{\frac{1}{c}}.\end{aligned}$$

Similarly, we have

$$\|\hat{P}_{\mu_2}(\xi)\hat{g}^{\delta}(\xi) - \hat{g}(\xi)\| \leq 2\delta + \tau\delta^{\frac{1}{c}}.$$

□

Lemma 5. *Assume that conditions (5) and (12) are satisfied. Then the following estimate holds:*

$$e^{\frac{p}{2\mu_1}}\delta^{\frac{1}{c}} \leq \frac{E_p}{\tau}, \quad e^{\frac{p}{2\mu_2}}\delta^{\frac{1}{c}} \leq \frac{E_p}{\tau}.$$

Proof. Applying the triangle inequality, we obtain

$$\begin{aligned}
\delta + \tau\delta^{\frac{1}{c}} &= \|(1 - \hat{P}_{\mu_1}(\xi))\hat{f}^{\delta}(\xi)\| \\
&\leq \|(1 - \hat{P}_{\mu_1}(\xi))(\hat{f}^{\delta}(\xi) - \hat{f}(\xi))\| + \|(1 - \hat{P}_{\mu_1}(\xi))\hat{f}(\xi)\| \\
&\leq \delta + \|(1 - \hat{P}_{\mu_1}(\xi))e^{-\frac{p}{2}|\xi|}e^{\frac{p}{2}|\xi|}\hat{f}(\xi)\| \\
&\leq \delta + \sup_{\xi\in\mathbb{R}^n} |(1 - \hat{P}_{\mu_1}(\xi))e^{-\frac{p}{2}|\xi|}|E_p \\
&\leq \delta + e^{-\frac{p}{2\mu_1}}E_p,
\end{aligned}$$

from which it follows that

$$e^{\frac{p}{2\mu_1}}\delta^{\frac{1}{c}} \leq \frac{E_p}{\tau}.$$

Similarly, we have

$$\begin{aligned}
\delta + \tau\delta^{\frac{1}{c}} &= \|(1 - \hat{P}_{\mu_2}(\xi))\hat{g}^{\delta}(\xi)\| \\
&\leq \|(1 - \hat{P}_{\mu_2}(\xi))(\hat{g}^{\delta}(\xi) - \hat{g}(\xi))\| + \|(1 - \hat{P}_{\mu_2}(\xi))\hat{g}(\xi)\| \\
&\leq \delta + \|(1 - \hat{P}_{\mu_2}(\xi))e^{-\frac{p}{2}|\xi|}e^{\frac{p}{2}|\xi|}\hat{g}(\xi)\| \\
&\leq \delta + \sup_{\xi\in\mathbb{R}^n} |(1 - \hat{P}_{\mu_2}(\xi))e^{-\frac{p}{2}|\xi|}|E_p \\
&\leq \delta + e^{-\frac{p}{2\mu_2}}E_p,
\end{aligned}$$

and hence

$$e^{\frac{p}{2\mu_2}}\delta^{\frac{1}{c}} \leq \frac{E_p}{\tau}.$$

□

Theorem 3. *Assume that $\hat{P}_{\mu}(\xi)$ is a truncated-kernel function and $w^{\mu,\delta}(x,\mathbf{y}) = u^{\mu_1,\delta}(x,\mathbf{y}) + v^{\mu_2,\delta}(x,\mathbf{y})$ denotes the regularized solution for $0 < x < 1$, where μ_1 and μ_2 are the solutions to Equations (15) and (16), respectively. If condition (5) is satisfied and condition (12) holds for $p = 2$, then the following error estimate holds:*

$$\|w^{\mu,\delta}(x,\cdot) - w(x,\cdot)\| \leq 2\delta^{\frac{1-x}{c}}(\tau + o(1))^{1-x}e^{kx}((\frac{E_2}{\tau})^c + E_2)^x.$$

Proof. Applying Parseval's identity, the Hölder inequality, Lemma 4, and Lemma 5, we obtain

$$\begin{aligned}
\|u^{\mu_1,\delta}(x,\cdot)-u(x,\cdot)\| &= \|\hat{u}^{\mu_1,\delta}(x,\cdot)-\hat{u}(x,\cdot)\| \\
&= \|(\hat{P}_{\mu_1}(\xi)\hat{f}^{\delta}(\xi)-\hat{f}(\xi))\cosh(x\sqrt{\xi^2+k^2})\| \\
&\le \|(\hat{P}_{\mu_1}(\xi)\hat{f}^{\delta}(\xi)-\hat{f}(\xi))\|^{1-x} \\
&\quad \cdot \|(\hat{P}_{\mu_1}(\xi)\hat{f}^{\delta}(\xi)-\hat{f}(\xi))(\cosh(x\sqrt{\xi^2+k^2}))^{\frac{1}{x}}\|^{x} \\
&\le \|(\hat{P}_{\mu_1}(\xi)\hat{f}^{\delta}(\xi)-\hat{f}(\xi))\|^{1-x}\|(\hat{P}_{\mu_1}(\xi)\hat{f}^{\delta}(\xi)-\hat{f}(\xi))e^{\sqrt{\xi^2+k^2}}\|^{x} \\
&\le (2\delta+\tau\delta^{\frac{1}{c}})^{1-x}(\|\hat{P}_{\mu_1}(\xi)(\hat{f}^{\delta}(\xi)-\hat{f}(\xi))e^{\sqrt{\xi^2+k^2}}\| \\
&\quad +\|(1-\hat{P}_{\mu_1}(\xi))\hat{f}(\xi)e^{\sqrt{\xi^2+k^2}}\|)^{x} \\
&\le (2\delta+\tau\delta^{\frac{1}{c}})^{1-x}(\sup_{\xi\in\mathbb{R}^n}|\hat{P}_{\mu_1}(\xi)e^{\sqrt{\xi^2+k^2}}|\delta \\
&\quad +\|(1-\hat{P}_{\mu_1}(\xi))\frac{e^{\sqrt{\xi^2+k^2}}}{e^{|\xi|}}e^{|\xi|}\hat{f}(\xi)\|)^{x} \\
&\le (2\delta+\tau\delta^{\frac{1}{c}})^{1-x}(e^{\frac{c}{\mu_1}}e^{k}\delta+e^{k}E_2)^{x} \\
&\le (2\delta+\tau\delta^{\frac{1}{c}})^{1-x}e^{kx}(e^{\frac{c}{\mu_1}}\delta+E_2)^{x} \\
&\le (2\delta+\tau\delta^{\frac{1}{c}})^{1-x}e^{kx}((\frac{E_2}{\tau})^{c}+E_2)^{x} \\
&= \delta^{\frac{1-x}{c}}(\tau+o(1))^{1-x}e^{kx}((\frac{E_2}{\tau})^{c}+E_2)^{x}.
\end{aligned}$$

Similarly, we obtain

$$\begin{aligned}
\|v^{\mu_2,\delta}(x,\cdot)-v(x,\cdot)\| &= \|\hat{v}^{\mu_2,\delta}(x,\cdot)-\hat{v}(x,\cdot)\| \\
&= \|(\hat{P}_{\mu_2}(\xi)\hat{g}^{\delta}(\xi)-\hat{g}(\xi))\frac{\sinh(x\sqrt{\xi^2+k^2})}{\sqrt{\xi^2+k^2}}\| \\
&\le \|(\hat{P}_{\mu_2}(\xi)\hat{g}^{\delta}(\xi)-\hat{g}(\xi))\cosh(x\sqrt{\xi^2+k^2})\| \\
&\le \delta^{\frac{1-x}{c}}(\tau+o(1))^{1-x}e^{kx}((\frac{E_2}{\tau})^{c}+E_2)^{x}.
\end{aligned}$$

Hence, the regularized solution $w^{\mu,\delta}(x,\mathbf{y})=u^{\mu_1,\delta}(x,\mathbf{y})+v^{\mu_2,\delta}(x,\mathbf{y})$ satisfies

$$\|w^{\mu,\delta}(x,\cdot)-w(x,\cdot)\| \le 2\delta^{\frac{1-x}{c}}(\tau+o(1))^{1-x}e^{kx}((\frac{E_2}{\tau})^{c}+E_2)^{x}.$$

□

Remark 2. *From Theorems 1 and 3, we know that the convergence rate of the regularized solution with an a priori parameter choice is* $O(\delta^{\frac{1-x}{1+(c-1)x}})$, *while that with an a posteriori parameter choice is* $O(\delta^{\frac{1-x}{c}})$. *The constant c, as defined in Definition 1, is equal to* 1 *for the Dirichlet kernel and* 2 *for other truncated-kernels. Therefore, the a priori convergence rate is identical to the a posteriori one for the Dirichlet kernel, whereas for other truncated-kernels, the a priori rate is superior to the a posteriori one.*

Next, we consider the case $x=1$, *where stronger additional assumptions on the exact data* $f(\mathbf{y})$ *and* $g(\mathbf{y})$ *are required.*

Theorem 4. *Assume that* $\hat{P}_{\mu}(\xi)$ *is a truncated-kernel function and* $w^{\mu,\delta}(1,\mathbf{y})=u^{\mu_1,\delta}(1,\mathbf{y})+v^{\mu_2,\delta}(1,\mathbf{y})$ *denotes the regularized solution at* $x=1$, *where* μ_1 *and* μ_2 *are the solutions to*

Equations (15) and (16), respectively. If condition (5) is satisfied and condition (12) holds for $p > 2$, then the following error estimate holds:

$$\|w^{\mu,\delta}(1,\cdot) - w(1,\cdot)\| \le 2\delta^{\frac{p-2}{pc}}(\tau + o(1))^{\frac{p-2}{p}} e^k((\frac{E_p}{\tau})^c + E_p)^{\frac{2}{p}}.$$

Proof. Applying Parseval's identity, the Hölder inequality, Lemma 4, and Lemma 5, we have

$$\begin{aligned}
\|u^{\mu_1,\delta}(1,\cdot) - u(1,\cdot)\| &= \|\hat{u}^{\mu_1,\delta}(1,\cdot) - \hat{u}(1,\cdot)\| \\
&= \|(\hat{P}_{\mu_1}(\xi)\hat{f}^\delta(\xi) - \hat{f}(\xi))\cosh(\sqrt{\xi^2+k^2})\| \\
&\le \|(\hat{P}_{\mu_1}(\xi)\hat{f}^\delta(\xi) - \hat{f}(\xi))\|^{\frac{p-2}{p}} \\
&\quad \cdot \|(\hat{P}_{\mu_1}(\xi)\hat{f}^\delta(\xi) - \hat{f}(\xi))(\cosh(\sqrt{\xi^2+k^2}))^{\frac{p}{2}}\|^{\frac{2}{p}} \\
&\le \|(\hat{P}_{\mu_1}(\xi)\hat{f}^\delta(\xi) - \hat{f}(\xi))\|^{\frac{p-2}{p}} \\
&\quad \cdot \|(\hat{P}_{\mu_1}(\xi)\hat{f}^\delta(\xi) - \hat{f}(\xi))e^{\frac{p}{2}\sqrt{\xi^2+k^2}}\|^{\frac{2}{p}} \\
&\le (2\delta + \tau\delta^{\frac{1}{c}})^{\frac{p-2}{p}}(\|\hat{P}_{\mu_1}(\xi)(\hat{f}^\delta(\xi) - \hat{f}(\xi))e^{\frac{p}{2}\sqrt{\xi^2+k^2}}\| \\
&\quad + \|(1 - \hat{P}_{\mu_1}(\xi))\hat{f}(\xi)e^{\frac{p}{2}\sqrt{\xi^2+k^2}}\|)^{\frac{2}{p}} \\
&\le (2\delta + \tau\delta^{\frac{1}{c}})^{\frac{p-2}{p}}(\sup_{\xi\in\mathbb{R}^n}|\hat{P}_{\mu_1}(\xi)e^{\frac{p}{2}\sqrt{\xi^2+k^2}}|\delta \\
&\quad + \|(1 - \hat{P}_{\mu_1}(\xi))\frac{e^{\frac{p}{2}\sqrt{\xi^2+k^2}}}{e^{\frac{p}{2}|\xi|}}e^{\frac{p}{2}|\xi|}\hat{f}(\xi)\|)^{\frac{2}{p}} \\
&\le (2\delta + \tau\delta^{\frac{1}{c}})^{\frac{p-2}{p}}(e^{\frac{pc}{2\mu_1}}e^{\frac{pk}{2}}\delta + e^{\frac{pk}{2}}E_p)^{\frac{2}{p}} \\
&\le (2\delta + \tau\delta^{\frac{1}{c}})^{\frac{p-2}{p}}e^k((\frac{E_p}{\tau})^c + E_p)^{\frac{2}{p}} \\
&= \delta^{\frac{p-2}{pc}}(\tau + o(1))^{\frac{p-2}{p}}e^k((\frac{E_p}{\tau})^c + E_p)^{\frac{2}{p}}.
\end{aligned}$$

Similarly, we obtain

$$\begin{aligned}
\|v^{\mu_2,\delta}(1,\cdot) - v(1,\cdot)\| &= \|\hat{v}^{\mu_2,\delta}(1,\cdot) - \hat{v}(1,\cdot)\| \\
&= \|(\hat{P}_{\mu_2}(\xi)\hat{g}^\delta(\xi) - \hat{g}(\xi))\frac{\sinh(\sqrt{\xi^2+k^2})}{\sqrt{\xi^2+k^2}}\| \\
&\le \|(\hat{P}_{\mu_2}(\xi)\hat{g}^\delta(\xi) - \hat{g}(\xi))\cosh(\sqrt{\xi^2+k^2})\| \\
&\le \delta^{\frac{p-2}{pc}}(\tau + o(1))^{\frac{p-2}{p}}e^k((\frac{E_p}{\tau})^c + E_p)^{\frac{2}{p}}.
\end{aligned}$$

Hence, the regularized solution $w^{\mu,\delta}(x,\mathbf{y}) = u^{\mu_1,\delta}(x,\mathbf{y}) + v^{\mu_2,\delta}(x,\mathbf{y})$ satisfies

$$\|w^{\mu,\delta}(1,\cdot) - w(1,\cdot)\| \le 2\delta^{\frac{p-2}{pc}}(\tau + o(1))^{\frac{p-2}{p}}e^k((\frac{E_p}{\tau})^c + E_p)^{\frac{2}{p}}.$$

□

Remark 3. *From Theorems 2 and 4, the convergence rate of the regularized solution with an a priori parameter choice is $O(\delta^{\frac{p-2}{2c+p-2}})$, while that with an a posteriori parameter choice is $O(\delta^{\frac{p-2}{pc}})$. As in the case $0 < x < 1$, the two rates are identical for the Dirichlet kernel, but the a priori rate is superior for other truncated-kernels.*

5. Numerical Experiments

In this section, we present several numerical examples to demonstrate the effectiveness of the mollification method with truncated-kernel. The numerical experiments are performed using MATLAB R2016b. Consider the two-dimensional case, and assume that the exact data $u(x,\mathbf{y}), v(x,\mathbf{y}), w(x,\mathbf{y})$, $x \in [0,1]$ is identically zero outside the domain $\mathbf{y} \in [-2\pi,2\pi]\times[-2\pi,2\pi]$. The domain $[-2\pi,2\pi]\times[-2\pi,2\pi]$ is partitioned into N^2 equal-area subregions, with a uniform sampling step of $\frac{4\pi}{N-1}$. The perturbed data f^δ are obtained by discretizing the exact data $f(\mathbf{y}) = u(0,\mathbf{y})$ on an $N \times N$ grid to get f, and then adding noise as

$$f^\delta = f + \epsilon \cdot \mathrm{rand}(\mathrm{size}(f)), \tag{18}$$

where rand$(\cdot)$ returns a matrix containing pseudorandom values drawn from the standard uniform distribution on the open interval $(0,1)$. The error level of the perturbed data f^δ is

$$\delta_f = \|f^\delta - f\| := \frac{4\pi}{N}\sqrt{\sum_{i,j=1}^{N}(f_{ij}^\delta - f_{ij})^2}.$$

The relative error of the regularized solution $u^{\mu,\delta}$ is

$$\mathrm{rel}(u^{\mu,\delta}) = \frac{\|u^{\mu,\delta}(x,\cdot) - u(x,\cdot)\|}{\|u(x,\cdot)\|}.$$

Following the same procedure, we obtain the perturbed data g^δ, the error level δ_g, and the relative error $\mathrm{rel}(v^{\mu,\delta})$. Since the *a priori* choice of the regularization parameter relies on an additional assumption on the exact data that is often difficult to verify in practice, we adopt the *a posteriori* choice strategy instead.

The numerical implementation proceeds as follows:

(1) A two-dimensional discrete Fourier transform (2D-DFT) is applied to the perturbed data f^δ or g^δ using MATLAB's built-in Fast Fourier Transform (FFT). The frequency domain is taken as $[-\frac{N-1}{4},\frac{N-1}{4}]\times[-\frac{N-1}{4},\frac{N-1}{4}]$ with a sampling step of $\frac{1}{2}$. In all numerical experiments, the grid parameter is set to $N = 129$.

(2) In the frequency domain, the transforms $\hat{u}^{\mu_1,\delta}$ or $\hat{v}^{\mu_2,\delta}$ of the regularized solutions are computed via (6) or (7). The regularization parameters μ_1 and μ_2 are selected independently via the a posteriori strategy, with each determined by solving the corresponding nonlinear equation, (15) for μ_1 and (16) for μ_2, using the bisection method on $(0,2)$. The solver employs a maximum of 100 iterations and a convergence tolerance of 10^{-6}, and the parameter τ in both equations is fixed at 0.1.

(3) Finally, a two-dimensional discrete inverse Fourier transform (2D-IDFT) is performed on $\hat{u}^{\mu,\delta}$ or $\hat{v}^{\mu,\delta}$ using MATLAB's IFFT, yielding the regularized solutions $u^{\mu,\delta}$ or $v^{\mu,\delta}$ in the spatial domain $[-2\pi,2\pi]\times[-2\pi,2\pi]$.

Example 1. *Consider the exact solution of (2) defined as*

$$u(x,\mathbf{y}) = u(x,y_1,y_2) = \sin(qy_1)\sin(qy_2)\cosh(x\sqrt{k^2+2q^2}).$$

Accordingly, the function $f(\mathbf{y})$ is given by

$$f(\mathbf{y}) = u(0,\mathbf{y}) = \sin(qy_1)\sin(qy_2).$$

For $q = \frac{1}{2}$, Tables 1–4 present the relative errors of the regularized solution $u^{\mu,\delta}$ obtained using the Dirichlet kernel, the Poussin kernel, the logarithmic kernel, and the

hyperbolic tangent kernel, respectively, for various values of ϵ, x, and k. Based on the data in Tables 1–4, the following conclusions can be drawn:

(1) As x increases, the ill-posedness of the Cauchy problem becomes more pronounced, resulting in larger errors in the corresponding regularized solution.

(2) As the noise level ϵ increases, the error in the corresponding regularized solution also increases consistently.

(3) The wave number k has a relatively minor influence on the accuracy of the regularized solution.

(4) The regularization performance of the Dirichlet kernel, the Poussin kernel, the logarithmic kernel, and the hyperbolic tangent kernel within the mollification method is comparable.

Table 1. The relative errors of the regularized solution $u^{\mu,\delta}$ with the Dirichlet kernel for $q = \frac{1}{2}$ and various values of ϵ, x, and k.

		$\epsilon = 0.001$	$\epsilon = 0.01$	$\epsilon = 0.1$
$x = 0.2$	$k = 1$	0.0108	0.0101	0.0994
	$k = 10$	0.0106	0.0107	0.1011
	$k = 100$	0.0106	0.0106	0.1013
$x = 0.5$	$k = 1$	0.0192	0.0194	0.0968
	$k = 10$	0.0110	0.0111	0.1010
	$k = 100$	0.0106	0.0106	0.1021
$x = 0.8$	$k = 1$	0.0498	0.0505	0.0895
	$k = 10$	0.0119	0.0120	0.1011
	$k = 100$	0.0106	0.0106	0.1007

Table 2. The relative errors of the regularized solution $u^{\mu,\delta}$ with the Poussin kernel for $q = \frac{1}{2}$ and various values of ϵ, x, and k.

		$\epsilon = 0.001$	$\epsilon = 0.01$	$\epsilon = 0.1$
$x = 0.2$	$k = 1$	0.0097	0.0100	0.1018
	$k = 10$	0.0099	0.0102	0.1045
	$k = 100$	0.0104	0.0103	0.1031
$x = 0.5$	$k = 1$	0.0141	0.0142	0.1020
	$k = 10$	0.0099	0.0101	0.1030
	$k = 100$	0.0101	0.0103	0.1022
$x = 0.8$	$k = 1$	0.0388	0.0428	0.1026
	$k = 10$	0.0098	0.0101	0.1026
	$k = 100$	0.0101	0.0102	0.1028

Table 3. The relative errors of the regularized solution $u^{\mu,\delta}$ with the logarithmic kernel for $m = 4$, $q = \frac{1}{2}$, and various values of ϵ, x, and k.

		$\epsilon = 0.001$	$\epsilon = 0.01$	$\epsilon = 0.1$
$x = 0.2$	$k = 1$	0.0099	0.0100	0.1007
	$k = 10$	0.0100	0.0101	0.1033
	$k = 100$	0.0102	0.0103	0.1021
$x = 0.5$	$k = 1$	0.0152	0.0153	0.1018
	$k = 10$	0.0097	0.0101	0.1024
	$k = 100$	0.0101	0.0102	0.1020
$x = 0.8$	$k = 1$	0.0415	0.0471	0.1018
	$k = 10$	0.0098	0.0099	0.1027
	$k = 100$	0.0101	0.0102	0.1019

Table 4. The relative errors of the regularized solution $u^{\mu,\delta}$ with the hyperbolic tangent kernel for $m = 4$, $q = \frac{1}{2}$, and various values of ϵ, x, and k.

		$\epsilon = 0.001$	$\epsilon = 0.01$	$\epsilon = 0.1$
$x = 0.2$	$k = 1$	0.0101	0.0101	0.1009
	$k = 10$	0.0102	0.0104	0.1022
	$k = 100$	0.0102	0.0102	0.1029
$x = 0.5$	$k = 1$	0.0176	0.0185	0.1021
	$k = 10$	0.0104	0.0105	0.1017
	$k = 100$	0.0103	0.0104	0.1029
$x = 0.8$	$k = 1$	0.0479	0.0497	0.1007
	$k = 10$	0.0111	0.0110	0.1030
	$k = 100$	0.0102	0.0102	0.1021

For both the logarithmic-type and hyperbolic tangent-type kernels, the parameter m governs the decay rate of the kernel over $|\xi| \in (\frac{1}{\mu}, \frac{2}{\mu})$; however, numerical experiments demonstrate that the influence of $m \in [2, 8]$ on the regularized solution is negligible. Thus, we fix $m = 4$ and exclude it from the set of sensitive parameters in subsequent analyses. For $\epsilon = 0.01$, the relative errors of the regularized solution $u^{\mu,\delta}$ with the Poussin kernel for various values of q, x, and k are reported in Table 5. These results demonstrate that regularization remains effective even when the exact solution $u(x, \mathbf{y})$ is highly oscillatory.

Table 5. The relative errors of the regularized solution $u^{\mu,\delta}$ with the Poussin kernel for $\epsilon = 0.01$ and various values of q, x, and k.

		$q = \frac{1}{2}$	$q = 1$	$q = 2$
$x = 0.2$	$k = 1$	0.0100	0.0196	0.0382
	$k = 10$	0.0102	0.0197	0.0389
	$k = 100$	0.0103	0.0204	0.0406
$x = 0.5$	$k = 1$	0.0142	0.0268	0.0461
	$k = 10$	0.0101	0.0193	0.0369
	$k = 100$	0.0103	0.0203	0.0402
$x = 0.8$	$k = 1$	0.0428	0.0668	0.0953
	$k = 10$	0.0101	0.0195	0.0364
	$k = 100$	0.0102	0.0201	0.0396

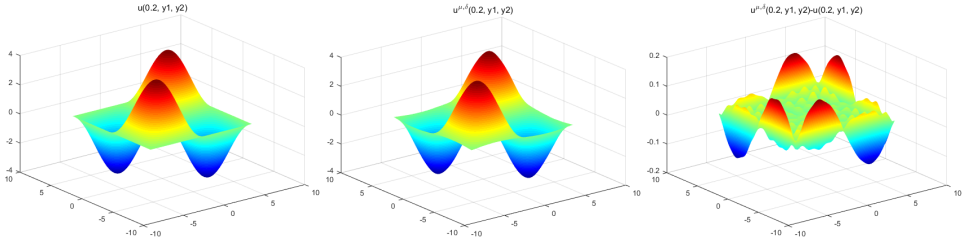
When $\epsilon = 0.01$, $q = \frac{1}{2}$, and $k = 10$, the exact solution $u(x, \mathbf{y})$ and the regularized solution $u^{\mu,\delta}(x, \mathbf{y})$ with the Poussin kernel at $x = 0.2, 0.5, 0.8$ are displayed in Figure 2, 3 and 4, respectively. Throughout this section, all surface plots use the default MATLAB parula colormap, where dark blue and red denote the minimum and maximum values, respectively, with intermediate values shown in a continuous gradient. As shown in Figures 2–4, the regularized solution provides a highly accurate approximation to the exact solution. Furthermore, the accuracy of the regularized solution increases as x decreases.

Example 2. *Consider the exact solution of (3) defined as*

$$v(x, \mathbf{y}) = v(x, y_1, y_2) = \cos(qy_1)\cos(qy_2)\frac{\sinh(x\sqrt{2q^2 + k^2})}{\sqrt{2q^2 + k^2}}.$$

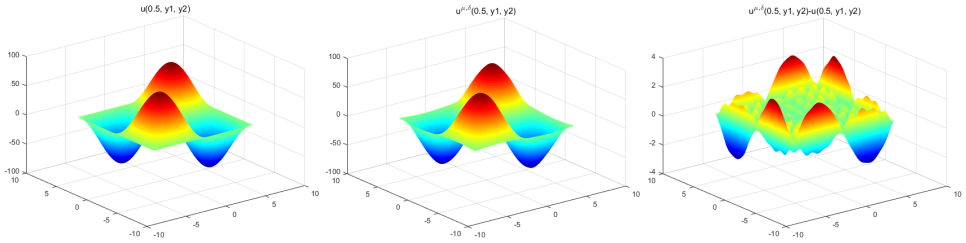
Accordingly, the function $g(\mathbf{y})$ is given by

$$g(\mathbf{y}) = v_x(0, \mathbf{y}) = \cos(qy_1)\cos(qy_2).$$



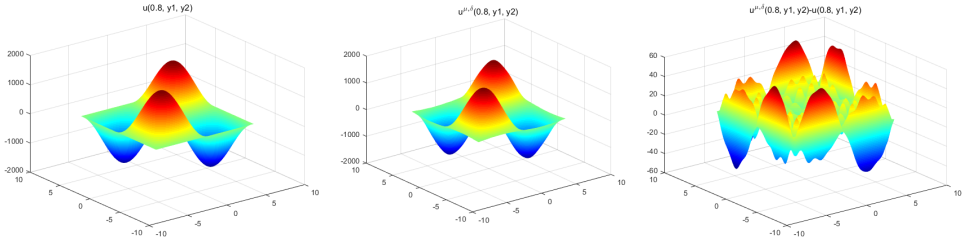
(**a**) $u(x, \mathbf{y})$ (**b**) $u^{\mu,\delta}(x, \mathbf{y})$ (**c**) $u^{\mu,\delta}(x, \mathbf{y}) - u(x, \mathbf{y})$

Figure 2. The exact solution $u(x, \mathbf{y})$, the regularized solution $u^{\mu,\delta}(x, \mathbf{y})$ with the Poussin kernel, and the error $u^{\mu,\delta}(x, \mathbf{y}) - u(x, \mathbf{y})$ at $x = 0.2$ when $\epsilon = 0.01$, $q = \frac{1}{2}$, and $k = 10$.



(**a**) $u(x, \mathbf{y})$ (**b**) $u^{\mu,\delta}(x, \mathbf{y})$ (**c**) $u^{\mu,\delta}(x, \mathbf{y}) - u(x, \mathbf{y})$

Figure 3. The exact solution $u(x, \mathbf{y})$, the regularized solution $u^{\mu,\delta}(x, \mathbf{y})$ with the Poussin kernel, and the error $u^{\mu,\delta}(x, \mathbf{y}) - u(x, \mathbf{y})$ at $x = 0.5$ when $\epsilon = 0.01$, $q = \frac{1}{2}$, and $k = 10$.



(**a**) $u(x, \mathbf{y})$ (**b**) $u^{\mu,\delta}(x, \mathbf{y})$ (**c**) $u^{\mu,\delta}(x, \mathbf{y}) - u(x, \mathbf{y})$

Figure 4. The exact solution $u(x, \mathbf{y})$, the regularized solution $u^{\mu,\delta}(x, \mathbf{y})$ with the Poussin kernel, and the error $u^{\mu,\delta}(x, \mathbf{y}) - u(x, \mathbf{y})$ at $x = 0.8$ when $\epsilon = 0.01$, $q = \frac{1}{2}$, and $k = 10$.

For $q = \frac{1}{4}$, Tables 6–9 present the relative errors of the regularized solution $v^{\mu,\delta}$ with the Dirichlet kernel, the Poussin kernel, the logarithmic kernel, and the hyperbolic tangent kernel, respectively, for various values of ϵ, x, and k. For $\epsilon = 0.01$, the relative errors of the regularized solution $u^{\mu,\delta}$ with the Poussin kernel for various values of q, x, and k are reported in Table 10. When $\epsilon = 0.01$, $q = \frac{1}{4}$, and $k = 10$, the exact solution $v(x, \mathbf{y})$ and the regularized solution $v^{\mu,\delta}(x, \mathbf{y})$ with the Poussin kernel at $x = 0.2, 0.5, 0.8$ are displayed in Figures 5, 6 and 7, respectively. These results are consistent with those observed in Example 1.

Building on Examples 1 and 2, we present the following numerical example.

Example 3. *Consider the Cauchy problem for the two-dimensional modified Helmholtz equation:*

$$\begin{cases} \Delta w(x, \mathbf{y}) - k^2 w(x, \mathbf{y}) = 0, \ \ 0 < x \leq 1, \ \ \mathbf{y} \in \mathbb{R}^2, \\ w(0, \mathbf{y}) = \sin(\frac{y_1}{4}) \sin(\frac{y_2}{4}), \ \ \mathbf{y} \in \mathbb{R}^2, \\ w_x(0, \mathbf{y}) = \cos(\frac{y_1}{2}) \cos(\frac{y_2}{2}), \ \ \mathbf{y} \in \mathbb{R}^2. \end{cases}$$

Table 6. The relative errors of the regularized solution $v^{\mu,\delta}$ with the Dirichlet kernel for $q = \frac{1}{4}$ and various values of ϵ, x, and k.

ϵ		**0.001**	**0.01**	**0.1**
$x = 0.2$	$k = 1$	0.0094	0.0144	0.1160
	$k = 10$	0.0094	0.0145	0.1152
	$k = 100$	0.0093	0.0146	0.1156
$x = 0.5$	$k = 1$	0.0126	0.0161	0.1112
	$k = 10$	0.0101	0.0144	0.1140
	$k = 100$	0.0093	0.0146	0.1157
$x = 0.8$	$k = 1$	0.0273	0.0284	0.1069
	$k = 10$	0.0118	0.0156	0.1122
	$k = 100$	0.0093	0.0145	0.1153

Table 7. The relative errors of the regularized solution $v^{\mu,\delta}$ with the Poussin kernel for $q = \frac{1}{4}$ and various values of ϵ, x, and k.

ϵ		**0.001**	**0.01**	**0.1**
$x = 0.2$	$k = 1$	0.0099	0.0152	0.1397
	$k = 10$	0.0102	0.0154	0.1395
	$k = 100$	0.0104	0.0156	0.1392
$x = 0.5$	$k = 1$	0.0113	0.0149	0.1368
	$k = 10$	0.0101	0.0144	0.1382
	$k = 100$	0.0102	0.0156	0.1435
$x = 0.8$	$k = 1$	0.0211	0.0235	0.1375
	$k = 10$	0.0108	0.0145	0.1377
	$k = 100$	0.0103	0.0155	0.1397

Table 8. The relative errors of the regularized solution $v^{\mu,\delta}$ with the logarithmic kernel for $m = 4$, $q = \frac{1}{4}$, and various values of ϵ, x, and k.

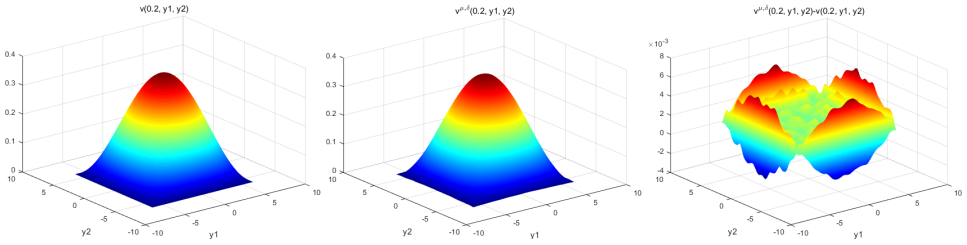
ϵ		**0.001**	**0.01**	**0.1**
$x = 0.2$	$k = 1$	0.0101	0.0151	0.1405
	$k = 10$	0.0104	0.0153	0.1409
	$k = 100$	0.0105	0.0154	0.1420
$x = 0.5$	$k = 1$	0.0119	0.0152	0.1399
	$k = 10$	0.0105	0.0146	0.1381
	$k = 100$	0.0103	0.0155	0.1423
$x = 0.8$	$k = 1$	0.0220	0.0243	0.1130
	$k = 10$	0.0113	0.0150	0.1393
	$k = 100$	0.0104	0.0152	0.1419

Table 9. The relative errors of the regularized solution $v^{\mu,\delta}$ with the hyperbolic tangent kernel for $m = 4$, $q = \frac{1}{4}$, and various values of ϵ, x, and k.

ϵ		**0.001**	**0.01**	**0.1**
$x = 0.2$	$k = 1$	0.0104	0.0153	0.1509
	$k = 10$	0.0107	0.0154	0.1514
	$k = 100$	0.0106	0.0157	0.1519
$x = 0.5$	$k = 1$	0.0130	0.0165	0.1474
	$k = 10$	0.0110	0.0152	0.1498
	$k = 100$	0.0104	0.0156	0.1525
$x = 0.8$	$k = 1$	0.0246	0.0269	0.1462
	$k = 10$	0.0123	0.0160	0.1487
	$k = 100$	0.0105	0.0153	0.1520

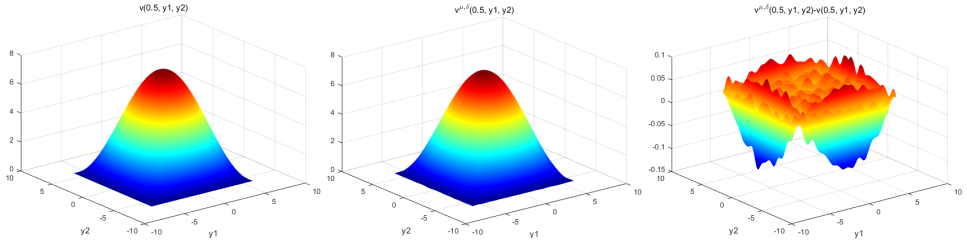
Table 10. The relative errors of the regularized solution $v^{\mu,\delta}$ with the Poussin kernel for $\epsilon = 0.01$ and various values of q, x, and k.

		$q = \frac{1}{4}$	$q = 1$	$q = 2$
$x = 0.2$	$k = 1$	0.0152	0.0170	0.0186
	$k = 10$	0.0154	0.0169	0.0192
	$k = 100$	0.0156	0.0166	0.0194
$x = 0.5$	$k = 1$	0.0149	0.0161	0.0171
	$k = 10$	0.0144	0.0165	0.0177
	$k = 100$	0.0156	0.0167	0.0197
$x = 0.8$	$k = 1$	0.0235	0.0157	0.0212
	$k = 10$	0.0145	0.0160	0.0169
	$k = 100$	0.0155	0.0169	0.0191



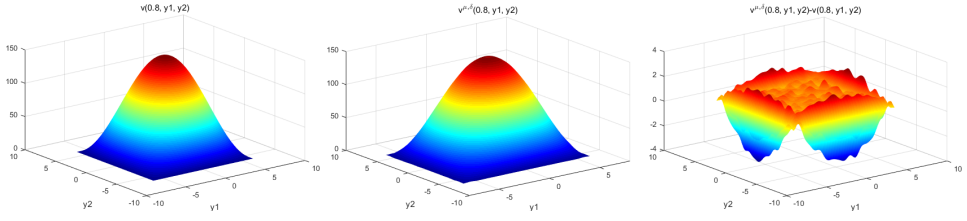
(a) $v(x, \mathbf{y})$ **(b)** $v^{\mu,\delta}(x, \mathbf{y})$ **(c)** $v^{\mu,\delta}(x, \mathbf{y}) - v(x, \mathbf{y})$

Figure 5. The exact solution $v(x, \mathbf{y})$, the regularized solution $v^{\mu,\delta}(x, \mathbf{y})$ with the Poussin kernel, and the error $v^{\mu,\delta}(x, \mathbf{y}) - v(x, \mathbf{y})$ at $x = 0.2$ when $\epsilon = 0.01$, $q = \frac{1}{4}$, and $k = 10$.



(a) $v(x, \mathbf{y})$ **(b)** $v^{\mu,\delta}(x, \mathbf{y})$ **(c)** $v^{\mu,\delta}(x, \mathbf{y}) - v(x, \mathbf{y})$

Figure 6. The exact solution $v(x, \mathbf{y})$, the regularized solution $v^{\mu,\delta}(x, \mathbf{y})$ with the Poussin kernel, and the error $v^{\mu,\delta}(x, \mathbf{y}) - v(x, \mathbf{y})$ at $x = 0.5$ when $\epsilon = 0.01$, $q = \frac{1}{4}$, and $k = 10$.



(a) $v(x, \mathbf{y})$ **(b)** $v^{\mu,\delta}(x, \mathbf{y})$ **(c)** $v^{\mu,\delta}(x, \mathbf{y}) - v(x, \mathbf{y})$

Figure 7. The exact solution $v(x, \mathbf{y})$, the regularized solution $v^{\mu,\delta}(x, \mathbf{y})$ with the Poussin kernel, and the error $v^{\mu,\delta}(x, \mathbf{y}) - v(x, \mathbf{y})$ at $x = 0.8$ when $\epsilon = 0.01$, $q = \frac{1}{4}$, and $k = 10$.

Table 11 present the relative errors of the regularized solution $w^{\mu,\delta}$ with the Poussin kernel for various values of ϵ, x, and k. When $\epsilon = 0.01$ and $k = 10$, the exact solution $w(x, \mathbf{y})$ and the regularized solution $w^{\mu,\delta}(x, \mathbf{y})$ with the Poussin kernel at $x = 0.2, 0.5, 0.8$ are displayed in Figures 8, 9 and 10, respectively. These results are consistent with those observed in Examples 1 and 2.

To further validate the method, we next examine a numerical example involving discontinuous exact solutions.

Example 4. *Consider the exact solution of (2) at $x = 1$ given by*

$$u(1, \mathbf{y}) = u(1, y_1, y_2) = \begin{cases} 10^4, & |y_1| + |y_2| \le 4, \\ 0, & |y_1| + |y_2| > 4. \end{cases}$$

The exact solution of (3) at $x = 1$ is

$$v(1, \mathbf{y}) = v(1, y_1, y_2) = u(1, y_1, y_2).$$

Consequently, the functions $f(\mathbf{y})$ and $g(\mathbf{y})$ are given respectively by

$$f(\mathbf{y}) = \frac{1}{2\pi} \int_{\mathbb{R}^2} \frac{\hat{u}(1, \xi)}{\cosh(\sqrt{|\xi|^2 + k^2})} \cdot e^{i\xi \cdot \mathbf{y}} \, d\xi,$$

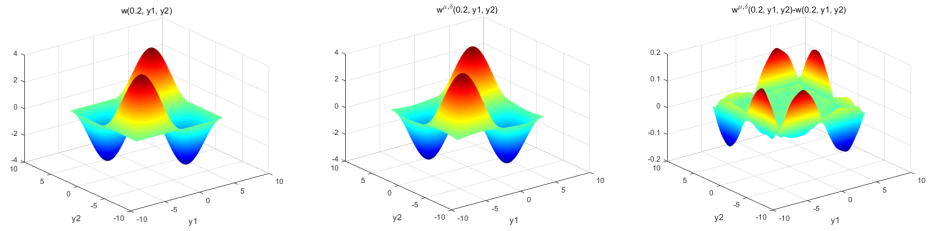
and

$$g(\mathbf{y}) = \frac{1}{2\pi} \int_{\mathbb{R}^2} \frac{\hat{v}(1, \xi) \sqrt{|\xi|^2 + k^2}}{\sinh(\sqrt{|\xi|^2 + k^2})} \cdot e^{i\xi \cdot \mathbf{y}} \, d\xi.$$

When $k = 10$, the exact data $f(\mathbf{y})$ and $g(\mathbf{y})$ are given in Figure 11; the perturbed data f^δ and g^δ are generated according to formula (18). When $k = 10$ and $x = 1$, Figure 12a presents the log-log plot of the relative error in f^δ versus that in the regularized solution $u^{\mu,\delta}$ obtained with the Poussin kernel, while Figure 12b shows the corresponding plot for g^δ and $v^{\mu,\delta}$. As demonstrated in Figure 12, the relative error of the regularized solution increases approximately linearly with the relative error of the perturbed data, indicating a power-law dependence between them. This observation is consistent with the theoretically predicted power-law convergence rate derived in this paper. When $k = 10$, the exact solution $u(1, \mathbf{y})$ and the regularized solution $u^{\mu,\delta}(1, \mathbf{y})$ obtained with the Poussin kernel are shown in Figure 13 for different noise levels. The corresponding results for $v(1, \mathbf{y})$ and $v^{\mu,\delta}(1, \mathbf{y})$ are presented in Figure 14. As demonstrated in Figures 13 and 14, the regularized solutions consistently capture the discontinuities present in the exact solution under various noise levels. These results confirm the effectiveness of the proposed approach for discontinuous problems.

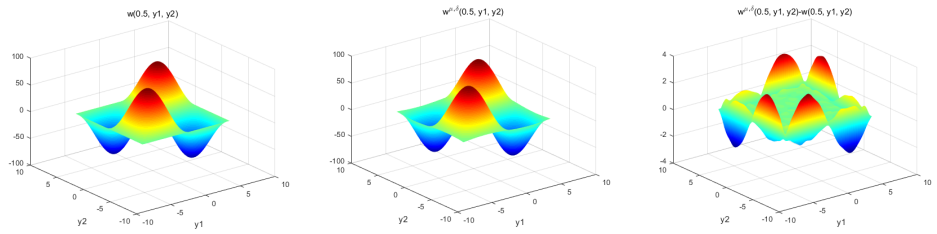
Table 11. The relative errors of the regularized solution $w^{\mu,\delta}$ with the Poussin kernel for various values of ϵ, x, and k.

ϵ		0.001	0.01	0.1
$x = 0.2$	$k = 1$	0.0099	0.0121	0.1223
	$k = 10$	0.0101	0.0112	0.1116
	$k = 100$	0.0103	0.0104	0.1029
$x = 0.5$	$k = 1$	0.0144	0.0146	0.1463
	$k = 10$	0.0097	0.0108	0.1089
	$k = 100$	0.0101	0.0104	0.1028
$x = 0.8$	$k = 1$	0.0443	0.0386	0.1553
	$k = 10$	0.0099	0.0107	0.1096
	$k = 100$	0.0101	0.0103	0.1029



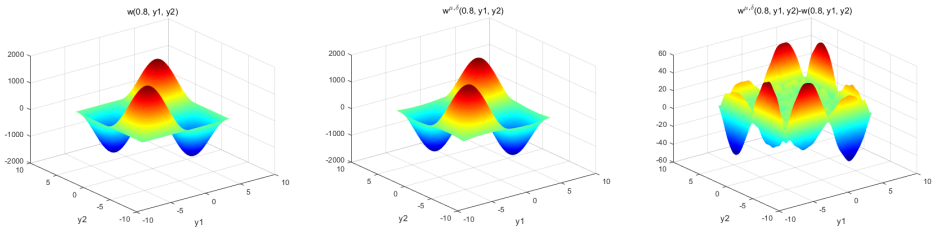
(a) $w(x, \mathbf{y})$ **(b)** $w^{\mu,\delta}(x, \mathbf{y})$ **(c)** $w^{\mu,\delta}(x, \mathbf{y}) - w(x, \mathbf{y})$

Figure 8. The exact solution $w(x, \mathbf{y})$, the regularized solution $w^{\mu,\delta}(x, \mathbf{y})$ with the Poussin kernel, and the error $w^{\mu,\delta}(x, \mathbf{y}) - w(x, \mathbf{y})$ at $x = 0.2$ when $\epsilon = 0.01$ and $k = 10$.



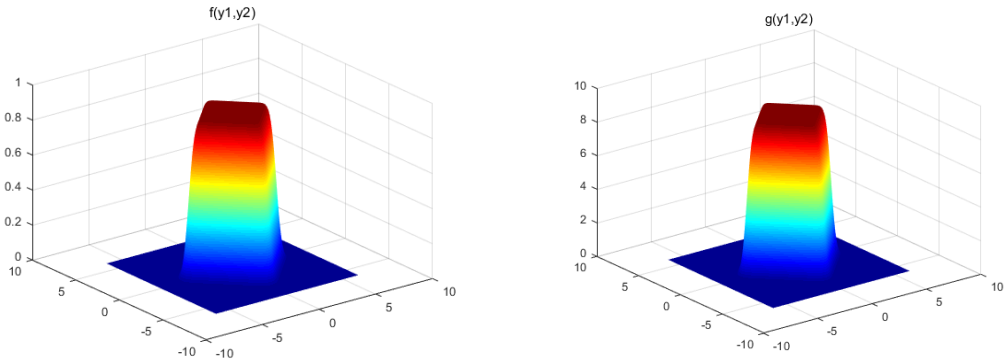
(**a**) $w\ (x, \mathbf{y})$ (**b**) $w^{\mu,\delta}(x, \mathbf{y})$ (**c**) $w^{\mu,\delta}(x, \mathbf{y}) - w\ (x, \mathbf{y})$

Figure 9. The exact solution $w(x, \mathbf{y})$, the regularized solution $w^{\mu,\delta}(x, \mathbf{y})$ with the Poussin kernel, and the error $w^{\mu,\delta}(x, \mathbf{y}) - w(x, \mathbf{y})$ at $x = 0.5$ when $\epsilon = 0.01$ and $k = 10$.



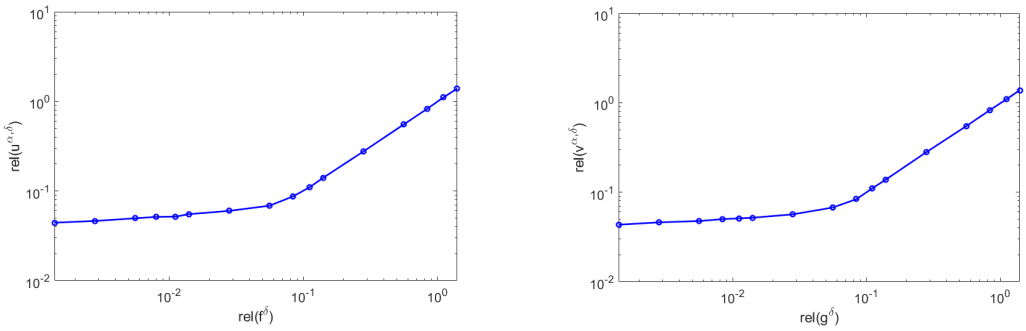
(**a**) $w\ (x, \mathbf{y})$ (**b**) $w^{\mu,\delta}(x, \mathbf{y})$ (**c**) $w^{\mu,\delta}(x, \mathbf{y}) - w\ (x, \mathbf{y})$

Figure 10. The exact solution $w(x, \mathbf{y})$, the regularized solution $w^{\mu,\delta}(x, \mathbf{y})$ with the Poussin kernel, and the error $w^{\mu,\delta}(x, \mathbf{y}) - w(x, \mathbf{y})$ at $x = 0.8$ when $\epsilon = 0.01$ and $k = 10$.



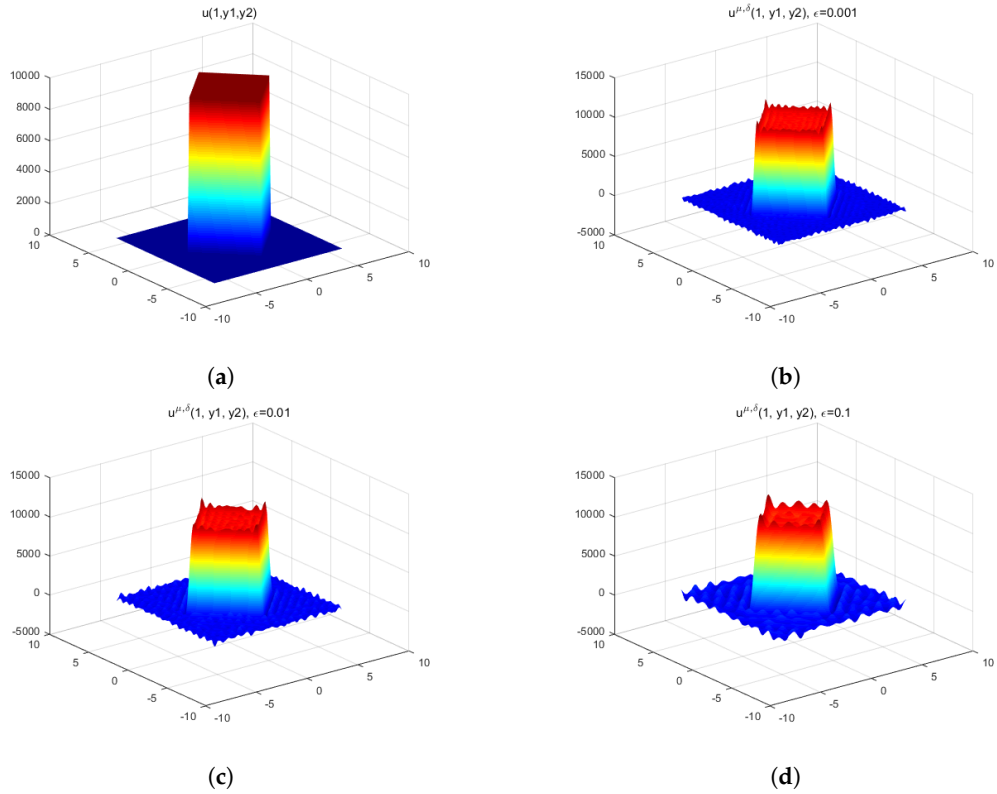
(**a**) $f(\mathbf{y})$ (**b**) $g(\mathbf{y})$

Figure 11. The exact data $f(\mathbf{y})$ and $g(\mathbf{y})$ in Example 4 for $k = 10$.



(**a**) $\text{rel}(f^{\delta})$ vs. $\text{rel}(u^{\mu,\delta})$ (**b**) $\text{rel}(g^{\delta})$ vs. $\text{rel}(v^{\mu,\delta})$

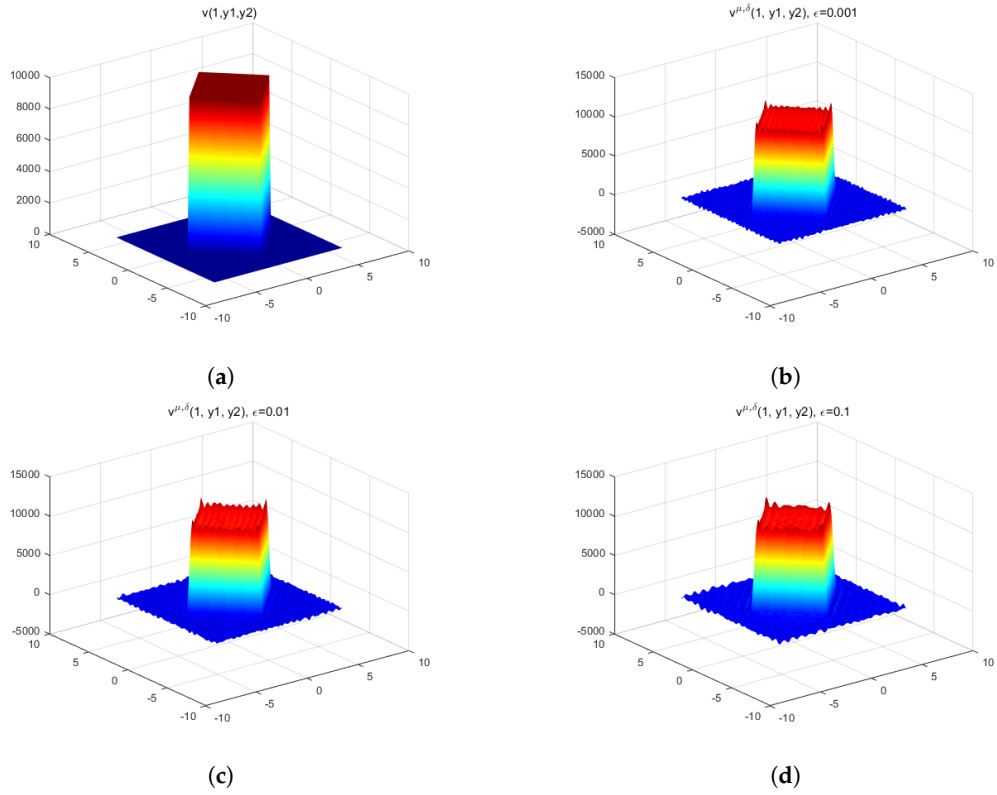
Figure 12. Log-log plots of relative errors for $k = 10$ and $x = 1$: (**a**) $\text{rel}(f^{\delta})$ vs. $\text{rel}(u^{\mu,\delta})$ and (**b**) $\text{rel}(g^{\delta})$ vs. $\text{rel}(v^{\mu,\delta})$.



(**a**) (**b**)

(**c**) (**d**)

Figure 13. The exact solution $u(1, \mathbf{y})$ (**a**) and the regularized solutions $u^{\mu,\delta}(1, \mathbf{y})$ with the Poussin kernel when $k = 10$, for noise levels $\epsilon = 0.001$ (**b**), 0.01 (**c**), and 0.1 (**d**).



(**a**) (**b**)

(**c**) (**d**)

Figure 14. The exact solution $v(1, \mathbf{y})$ (**a**) and the regularized solutions $v^{\mu,\delta}(1, \mathbf{y})$ with the Poussin kernel when $k = 10$, for noise levels $\epsilon = 0.001$ (**b**), 0.01 (**c**), and 0.1 (**d**).

6. Conclusions

In this paper, we propose a truncated-kernel mollification method to address the Cauchy problem of a multi-dimensional modified Helmholtz equation. Both *a priori* and *a posteriori* strategies for choosing the regularization parameters are introduced. Under additional assumptions on the exact data $f(\mathbf{y})$ and $g(\mathbf{y})$, error estimates for the regularized solutions are derived, and their convergence rates are analyzed. For the Dirichlet kernel, the *a posteriori* parameter choice achieves the same convergence order as the *a priori* strategy: $O(\delta^{1-x})$ for $0 < x < 1$, and $O(\delta^{\frac{p-2}{p}})$ for $x = 1$. In contrast, this property does not hold for other truncated kernels: although they also yield power-law convergence rates, the *a priori* strategy achieves a strictly higher rate than the *a posteriori* strategy. Numerical experiments demonstrate that the regularization performance of different truncated-kernels in the mollification method is comparable, and that the proposed method yields excellent reconstruction performance for both continuous and discontinuous exact solutions. Moreover, the wave number k has a relatively minor influence on the error of the regularized solutions.

Author Contributions: Conceptualization, H.X.; methodology, H.X.; software, F.X. and B.W.; validation, F.X. and B.W.; formal analysis, H.X.; investigation, H.X. and F.X.; resources, H.X.; data curation, F.X. and B.W.; writing—original draft preparation, H.X. and F.X.; writing—review and editing, H.X.; visualization, F.X. and B.W.; supervision, H.X.; project administration, H.X.; funding acquisition, H.X. All authors have read and agreed to the published version of the manuscript.

Funding: This research was funded by the National Natural Science Foundation of China (Grant No. 11661008).

Data Availability Statement: Data are contained within the article.

Conflicts of Interest: The authors declare no conflicts of interest.

References

1. Colton, D.; Kress, R. *Inverse Acoustic and Electromagnetic Scattering Theory*, 4th ed.; Springer: Cham, Switzerland, 2019.
2. Alessandrini, G.; Vessella, S. Lipschitz stability for the inverse conductivity problem. *Adv. Appl. Math.* **2005**, *35*, 207–241. [CrossRef]
3. Xiong, X.T.; Shi, W.X.; Fan, X.Y. Two numerical methods for a Cauchy problem for modified Helmholtz equation. *Appl. Math. Model.* **2011**, *35*, 4951–4964. [CrossRef]
4. Qin, H.H.; Wei, T. Quasi-reversibility and truncation methods to solve a Cauchy problem of the modifed Helmholtz equation. *Math. Comput. Simul.* **2009**, *80*, 352–366. [CrossRef]
5. Nguyen, H.T.; Tran, Q.V.; Nguyen, V.T. Some remarks on a modified Helmholtz equation with inhomogeneous source. *Appl. Math. Model.* **2013**, *37*, 793–814. [CrossRef]
6. Qian, A.L.; Yang, X.M.; Wu, Y.S. Optimal error bound and a quasi-boundary value regularization method for a Cauchy problem of the modified Helmholtz equation. *Int. J. Comput. Math.* **2015**, *93*, 2028–2041. [CrossRef]
7. Qin, H.H.; Wen, D.W. Tikhonov type regularization method for the Cauchy problem of the modified Helmholtz equation. *Appl. Math. Comput.* **2008**, *203*, 617–628. [CrossRef]
8. Zhang, H.W.; Zhang, X.J. Generalized Tikhonov method and convergence estimate for the Cauchy problem of modified Helmholtz equation with nonhomogeneous Dirichlet and Neumann datum. *Mathematics* **2019**, *7*, 667. [CrossRef]
9. Jday, F.; Omri, H. Adaptive Runge-Kutta regularization for a Cauchy problem of a modified Helmholtz equation. *J. Inverse III-Posed Probl.* **2023**, *31*, 351–374. [CrossRef]
10. Hamdi, H.; Nachaoui, M.; Bergam, A.; Nachaoui, A. A posteriori-driven adaptive strategy for solving inverse Cauchy problems in diffusion-reaction models. *Appl. Math. Comput.* **2026**, *518*, 129902. [CrossRef]
11. Chen, Y.G.; Yang, F.; Ding, Q. The Landweber Iterative Regularization Method for Solving the Cauchy Problem of the Modified Helmholtz Equation. *Symmetry* **2022**, *14*, 1209. [CrossRef]
12. Fu, C.L.; Feng, X.L.; Qian, Z. The Fourier regularization for solving the Cauchy problem for the Helmholtz equation. *Appl. Numer. Math.* **2009**, *59*, 2625–2640. [CrossRef]
13. He, S.Q.; Feng, X.F. A regularization method to solve a Cauchy problem for the two-dimensional modified Helmholtz equation. *Mathematics* **2019**, *7*, 360. [CrossRef]

14. Xu, H.L.; Wang, B.X.; Zhou, D.M. A general mollification regularization method to solve a Cauchy problem for the multi-dimensional modified Helmholtz equation. *Symmetry* **2024**, *16*, 1549. [CrossRef]
15. Hao, D.N. A mollification method for ill-posed problems. *Numer. Math.* **1994**, *68*, 469–506. [CrossRef]
16. Yang, L.; Zhu, L.; He, S.Q.; Feng, X.F.; Zhao, B.X. Solving two kinds of inverse source problems for the heat equations by a mollification regularization method with Dirichlet kernel. *Math. Methods Appl. Sci.* **2024**, *47*, 14024–14036. [CrossRef]
17. Yang, F.; Fu, C.L. A mollification regularization method for the inverse spatial-dependent heat source problem. *J. Comput. Appl. Math.* **2014**, *255*, 555–567. [CrossRef]
18. Qiao, Y.; Xiong, X.T.; Han, J.J. A variational approach to recover the unknown source and initial condition for a time-space fractional diffusion equation. *J. Appl. Math. Comput.* **2025**, *71*, 3445–3476. [CrossRef]
19. Yang, L.; Zhu, L.; He, S.Q.; Zhao, B.X. Regularization of the time-fractional order Schrödinger problem by using the mollification regularization method. *Math. Methods Appl. Sci.* **2025**, *48*, 6799–6817. [CrossRef]
20. Xu, H.L.; Xu, F.L.; Zhou, D.M.; Zhang, R. The mollification regularization method with truncated kernels for solving the inverse time-fractional Schrödinger problem. *Fractal Fract.* **2026**, *10*, 191. [CrossRef]
21. Maréchal, P.; Triki, F.; Lee, W. Regularization of the inverse Laplace transform by mollification. *Inverse Probl.* **2024**, *40*, 025010. [CrossRef]
22. Lee, W. A variational technique of mollification applied to backward heat conduction problems. *Appl. Math. Comput.* **2023**, *449*, 127917. [CrossRef]
23. Qiao, Y.; Xiong, X.T. A mollifier approach to the simultaneous identification of the unknown source and initial distribution in a space-fractional diffusion equation. *Appl. Math. Comput.* **2025**, *489*, 129175. [CrossRef]
24. Kirsch, A. *An Introduction to the Mathematical Theory of Inverse Problems*, 3rd ed.; Springer: Cham, Switzerland, 2021.

Disclaimer/Publisher's Note: The statements, opinions and data contained in all publications are solely those of the individual author(s) and contributor(s) and not of MDPI and/or the editor(s). MDPI and/or the editor(s) disclaim responsibility for any injury to people or property resulting from any ideas, methods, instructions or products referred to in the content.